THE JOURNAL OF PHYSICAL CHEMISTRY B

ARTICLE

pubs.acs.org/JPCB

Comparison of United-Atom Potentials for the Simulation of Vapor−Liquid Equilibria and Interfacial Properties of Long-Chain *n*-Alkanes up to *n*-C_{100}

Erich A. Müller* and Andrés Mejía*,†

Department of Chemical Engineering, Imperial College London, South Kensington Campus, London SW7 2AZ, United Kingdom

Supporting Information

ABSTRACT: Canonical ensemble molecular dynamics (MD) simulations are reported which compute both the vapor−liquid equilibrium properties (vapor pressure and liquid and vapor densities) and the interfacial properties (density profiles, interfacial tensions, entropy and enthalpy of surface formation) of four long-chained *n*-alkanes: *n*-decane (*n*-C_{10}), *n*-eicosane (*n*-C_{20}), *n*-hexacontane (*n*-C_{60}), and *n*-decacontane (*n*-C_{100}). Three of the most commonly employed united-atom (UA) force fields for alkanes (SKS: Smit, B.; Karaborni, S.; Siepmann, J. I. *J. Chem. Phys.* **1995,** *102*, 2126−2140; *J. Chem. Phys.* **1998,** *109*, 352; NERD: Nath, S. K.; Escobedo, F. A.; de Pablo, J. J. *J. Chem. Phys.* **1998**, *108*, 9905−9911; and TraPPE: Martin M. G.; Siepmann, J. I. *J. Phys. Chem. B* **1998**, *102*, 2569−2577.) are critically appraised. The computed results have been compared to the available experimental data and those fitted using the square gradient theory (SGT). In the latter approach, the Lennard−Jones chain equation of state (EoS), appropriately parametrized for long hydrocarbons, is used to model the homogeneous bulk phase Helmholtz energy. The MD results for phase equilibria of *n*-decane and *n*-eicosane exhibit sensible agreement both to the experimental data and EoS correlation for all potentials tested, with the TraPPE potential showing the lowest deviations. However, as the molecular chain increases to *n*-hexacontane and *n*-decacontane, the reliability of the UA potentials decreases, showing notorious subpredictions of both saturated liquid density and vapor pressure. Based on the recommended data and EoS results for the heaviest hydrocarbons, it is possible to attest, that in this extreme, the TraPPE potential shows the lowest liquid density deviations. The low absolute values of the vapor pressure preclude the discrimination among the three UA potentials studied. On the other hand, interfacial properties are very sensitive to the type of UA potential thus allowing a differentiation of the potentials. Comparing the interfacial tension MD results to the available experimental data and SGT results, the TraPPE model exhibits the lowest deviations for all hydrocarbons.

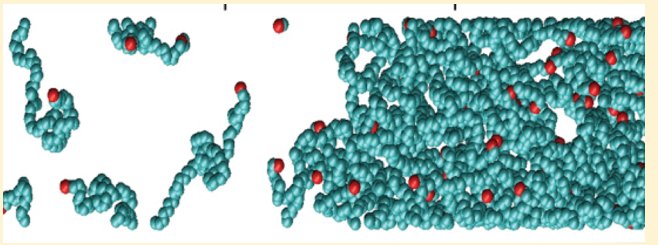

1. INTRODUCTION

Long *n*-alkanes (i.e., *n*-decane or larger) are ubiquitous in mixtures of practical importance in the petrochemical industry, being the major components in fuels, oils, waxes, paraffins, solvents, etc.,[1] and are key in many biological and environmentally related systems.[2] In all of these situations, vapor−liquid equilibria (VLE) along with the related interfacial properties play a central role in the performance and control of processes that occur between bulk phases that are in contact through a fluid interface. Some specific examples are mass transfer and chemical reactions between species, the wettability between fluid−fluid and fluid−solid phases, nucleation and coalescence, and emulsion formulation and stability, to name only a salient few.

Before attempting to describe both bulk phases and interfacial properties of mixtures that involve long *n*-alkanes, it is imperative to have confidence in our ability to characterize the phase and interface behavior of their constitutive pure fluids. For the case of long hydrocarbons (herein understood as linear *n*-alkanes longer than *n*-decane), experimental determination of vapor−liquid coexistence and interfacial tensions (IFT) becomes extremely difficult since the melting temperature increases with carbon number approaching the limit of thermal stability (c.a. 650 K). In fact, reliable experimental VLE and IFT data are only available up to *n*-dodecane ($C_{12}H_{26}$). For the case of heavier *n*-alkanes, from *n*-tridecane ($C_{13}H_{28}$) to *n*-decacontane ($C_{100}H_{202}$), no experimental data for vapor phase is available and some disperse and sometimes conflicting experimental data for vapor pressure, liquid densities, and interfacial tensions can be found in the literature.[3−6] Additionally, at low temperatures, some traces of solid phases may be present in the experimental apparatus inducing spurious results.

In order to overcome these experimental limitations, molecular simulations can provide complementary routes to obtain, over a broad temperature range, thermo-physical properties of interest, and thus become a means to rationally extrapolate the available low-temperature, low- molecular mass experimental

Received: April 7, 2011
Revised: September 20, 2011
Published: September 20, 2011

data. A textbook example was the use by Siepmann et al.[7] of simulations to discriminate between conflicting data sets in the literature describing the trend of the critical density of long *n*-alkanes with carbon number. Molecular simulations, based on Monte Carlo (MC) or molecular dynamics (MD) schemes, have been used to describe VLE[8−11] and IFT[12−20] or both,[21,22] in some cases up to *n*-octatetracontane ($C_{48}H_{98}$). However, the united atom (UA) force fields used above rely heavily on the assumption of transferability, i.e. on the premise that the parameters fitted to a given UA in a molecule may be used for any occurrence of the same group in another unrelated molecule. Another underlying assumption is that of representability, that the parameters that best fit a UA group for the prediction of a given property, say liquid density, are the same ones that adequately represent other properties not included in the fit, such as transport properties[23] or vapor pressures. It can be shown that most common fitting techniques employed will fail to address simultaneously the issues of transferability and representability. In spite of this, UA potentials are frequently used to correlate, and most worryingly, to predict the fluid phase behavior without due awareness of their limitations.

The main goal of this work is to provide an assessment and a guide to the merits and shortfalls of the most common intermolecular potentials available for the atomistic simulation of long alkanes. For this purpose we combine simulations, theory, and available experimental or recommended data to describe the VLE behavior (e.g., coexistence curve in terms of temperature, liquid and vapor densities, vapor pressure, and critical properties) and interfacial properties (e.g., density profiles along the interfacial region, interfacial tensions, surface entropy, and surface enthalpy change of surface formation) for the case of four long *n*-alkanes, namely *n*-decane ($C_{10}H_{22}$), *n*-eicosane ($C_{20}H_{42}$), *n*-hexacontane ($C_{60}H_{122}$) and *n*-decacontane ($C_{100}H_{202}$). As we exemplified in our recent paper,[24] this trilogy—simulation, theory, and experimentation—gives a very complete and complementary picture of bulk and interfacial properties of fluids. This paper is organized as follows; we first summarize the united atom potential models and the simulation techniques used to calculate the properties of interest (section 2). We then present the main expressions of the square gradient theory, the EoS model and a new set of molecular parameters used to correlate the behavior of long *n*-alkanes (section 3). Following, we present and discuss the main results of both equilibrium bulk phases and interfacial properties in section 4. We summarize the main conclusions of this work in section 5.

2. MOLECULAR DYNAMICS SIMULATIONS

Molecular simulations for hydrocarbons can be performed by using MC or MD schemes. There are some advantages of the latter method when considering larger molecules and/or when there is interest in retaining the interface region within the simulation box. Large-scale parallelization, which comes about naturally in MD simulations, results in a significant reduction of the computer time. Hence MD is the method of choice herein. We employ here canonical simulations where N molecules at a fixed temperature T are placed in a parallelepiped simulation cell of a constant volume V. Following to the standard MD methodology,[25,26] the N molecules that conform each hydrocarbon interact with each other according to an intermolecular potential. In this work, the hydrocarbons fluids are modeled using UA potential. The purpose of this coarse-graining is to reduce the computational effort, as MD simulations scale, at best, with the number of interaction sites. For a linear hydrocarbon of n carbons, C_nH_{2n+2}, is represented by n sites in the UA potential which is 3-fold less the sites needed in an all-atom scheme.

2.1. United Atom Potential Models. Three of the most common UA parametrizations for *n*-alkanes have been considered herein, namely those by Smit et al.[8] (SKS), Nath et al.[9] (NERD), and Martin and Siepmann[10] (TraPPE). For specific details, the reader is referred to their original papers. In these models, the intramolecular potential is given by the sum of three terms: nonbonded, bending, and torsion. Additionally, in the TraPPE as well as in the SKS models, there is a rigid bond between two consecutive united-atoms with a length of 1.54 Å for TraPPE model and 1.53 Å for SKS model. It is important to point out that in the original SKS model[7] the rigid bond distance was fixed at 1.54 Å. However, recent MD works where phase and interfacial behavior are simultaneously simulated (see for instance Nicolas and Smit[13] and Alejandre et al.[27]) use a value of 1.53 Å. In order to quantify the effect that this variable has on the results, we ran simulations for the phase equilibria and interfacial tension of decane using the two reported bond length values (1.53 and 1.54 Å). The results suggest that the small variation in this parameter has little impact on the results. A bond length of 1.53 Å seems to produce results which are more in line with the experimental data and is the value used here. For the case of NERD model, this bond is treated as a harmonic potential[28]

$$U(r) = \frac{k_r}{2}(r_{ij} - r_0)^2 \tag{1}$$

where r_{ij} is the bond distance between two united-atoms. The subscript 0 denotes its equilibrium value, and k_r is the spring constant. The constants in eq 1 are r_0 =1.54 Å, and k_r/k_B = 96 500 K/Å^2, and k_B is Boltzmann's constant. The bond bending interactions are modeled in terms of a harmonic potential[29]

$$U(\theta) = \frac{k_\theta}{2}(\theta - \theta_0)^2 \tag{2}$$

where θ is the bond angle between three consecutive united-atoms, subscript 0 denotes its equilibrium value, and k_θ is the spring constant. Here θ_0 = 114.0° and k_θ/k_B = 62 500 K/rad^2.

The torsional potential is modeled as a Fourier series in all cases, and it is given by[30]

$$U(\phi) = c_1(1 + \cos\phi) + c_2(1 - \cos 2\phi) + c_3(1 + \cos 3\phi) \tag{3}$$

where ϕ is the dihedral angle between four consecutive united-atoms, and c_1/k_B = 355.0 K, c_2/k_B = −68.19 K, and c_3/k_B = 791.3 K. Finally, the interaction between two united-atoms in different molecules or separated by more than three bonds within a molecule is given by a Lennard-Jones potential

$$U(r_{ij}) = 4\varepsilon_{ij}[(\sigma_{ij}/r_{ij})^{12} - (\sigma_{ij}/r_{ij})^6] \tag{4}$$

where r_{ij} is the distance between united-atoms i and j. ε_{ij} is the energy parameter of the interaction, whereas σ_{ij} is the Lennard-Jones size parameter. Unlike interactions are calculated by using the Lorentz−Berthelot mixing rules

$$\varepsilon_{ij} = \sqrt{\varepsilon_{ii}\varepsilon_{jj}}, \quad \sigma_{ij} = (\sigma_{ii} + \sigma_{jj})/2 \tag{5}$$

The fundamental differences among the different UA potentials considered are the values of the Lennard-Jones parameters

for each united atom (CH_3 and CH_2). For the SKS potential,[8] ε_{CH_3}/k_B = 114 K, ε_{CH_2}/k_B = 47 K, and $\sigma_{CH_3} = \sigma_{CH_2}$ = 3.93 Å; for the NERD potential,[9] ε_{CH_3}/k_B = 104 K, ε_{CH_2}/k_B = 45.8 K, and σ_{CH_3} = 3.91 Å, σ_{CH_2} = 3.93 Å; and for the TraPPE potential,[10] ε_{CH_3}/k_B = 98 K, ε_{CH_2}/k_B = 46 K, and σ_{CH_3} = 3.75 Å, σ_{CH_2} = 3.95 Å.

2.2. Simulation Details. MD simulations are performed on pure fluids containing at least 7000 UA sites at conditions where the liquid vapor interface is present. In this work, all simulations are started from a high temperature homogeneous one-phase system that was quenched instantaneously to the simulation temperature.[31] The simulation cell is a $L_x \times L_y \times L_z$ parallelepiped with periodic boundary conditions in all three directions. Here $L_x = L_y$ = 48 Å and L_z = 5 L_x except for the simulation of n-decacontane where L_z = 10 L_x. These values are chosen in order to accommodate enough molecules to ensure sensible-sized bulk phases and the corresponding two interfacial regions. We have observed that smaller systems tend to promote oscillations in the vapor pressure and interfacial tension results.[32,33] Since L_z is much larger than L_x and L_y, the interface spontaneously appears in the $x-y$ plane in an effort from the system to minimize its free energy. In all simulations based on NERD and TraPPE potential, we use a cutoff radius of 24 Å ($\sim 6\,\sigma$) in order to reduce the truncation and system size effects which could have an influence on the phase equilibrium and interfacial tension calculations (see refs 34−38 for a complete discussion of truncation effects). For the SKS potential we use the originally suggested cutoff radius of 13.8 Å, for which the parameters were fitted. The use of a larger cutoff radius actually produces an over prediction for both phase equilibria and interfacial tension. This point is expanded in the Supporting Information.

In this work all simulations are performed using the DL_POLY package 2.18[39] which incorporates force-decomposition algorithms allowing efficient parallelization with a small number of processors (typically 8). We employed the canonical *NVT* ensemble using a Nosé - Hoover thermostat with a relaxation constant of 1.0 ps and a Verlet leapfrog algorithm with a time step of 0.003 ps. After the initial temperature quenching, the systems are equilibrated for 15 ns. After this equilibration stage, a production run at least another 25 ns is performed. The corresponding statistics are accumulated every 5000 time steps.

Density profiles are calculated by dividing the system in 250 slabs along the z direction. The molecular density profiles, $\rho_i(z)$, are obtained by assigning the position of each united atom center, z_i, to the corresponding slab and constructing the molecular density from mass balance considerations. Additionally, these profiles (not the actual molecules) are displaced so that the center of mass of the liquid slab lies at the center of the simulation cell. This displacement helps to avoid smearing of the profiles due to fluctuations of the center of mass.

2.3. Vapor Pressure and Interfacial Tension Using the Irving−Kirkwood Method. The profiles of the pressure tensor diagonal elements are calculated by the Irving−Kirkwood method[25,26,40]

$$P_{\alpha\alpha} = k_B T N_{av} \rho(z) + \frac{1}{A}\left\langle \sum_{i}^{N-1} \sum_{j>i}^{N} \frac{1}{|z_i - z_j|} (f_{ij})_\alpha (r_{ij})_\alpha \right\rangle \quad (6)$$

In eq 6, $P_{\alpha\alpha}$ are the pressure tensor elements, where the subscript $\alpha\alpha$ represents the spatial coordinate, either x, y,or z. N_{av} is Avogadro's constant, A is the interfacial area, N is the number of molecules, f_{ij} is the force on molecule i due to molecule j, and r_{ij} represents the distance between molecules i and j. Both f_{ij} and r_{ij} contributions have been equally distributed along the simulation cell. In eq 6, the first term represents the ideal gas pressure (the kinetic contribution), whereas the second term corresponds to the configurational part, which is evaluated as ensemble averages, $\langle\rangle$

From the pressure elements of eq 6, one extracts the vapor pressure, corresponding to the P_{zz} element, whereas the interfacial tension, γ, between the liquid and vapor bulk phases can be calculated by integration

$$\gamma = \frac{1}{2}\int_{-\infty}^{+\infty} \left[P_{zz}(z) - \frac{P_{xx}(z) + P_{yy}(z)}{2} \right] dz \quad (7)$$

In this latter equation, the additional factor, 1/2, comes from having two interfaces in the system. Specific details related to the technical implementation of the previous expressions and their evaluation have been discussed extensively in the literature (e.g., see refs 34, 37, and 41.). This method has been used with no prejudice toward the test-area method,[42−44] which has been used to validate and test the implementation presented here.

2.4. Estimation of Critical State from Molecular Dynamics Results. Organic molecules are thermally unstable at temperatures higher than 650 K. Therefore; the experimental determination of their critical state is extremely difficult. However, the critical points of molecules are extensively employed in engineering correlations that invoke the corresponding states principle. In order to gain some insight in this direction, we use vapor−liquid equilibrium MD results together with scaling laws[45] in order to estimate the critical state for the heavy hydrocarbons. According to these scaling laws, the densities of coexisting liquid (ρ^L) and vapor phases (ρ^V) are related to the critical temperature (T_c) by

$$\rho^L - \rho^V = B(T - T_c)^{0.325} \quad (8)$$

In this equation, B and T_c are two unknown constants, found by fitting the difference between the densities of coexisting liquid and vapor phases with the temperature. Using the value of T_c, it is possible to calculate the critical density (ρ_c) and the critical pressure (P_c) by applying the "law" of rectilinear diameters and Clapeyron equation, respectively[45,46]

$$\frac{\rho^L + \rho^V}{2} = \rho_c + C(T - T_c) \quad (9)$$

$$\ln P = D + \frac{E}{T} \quad (10)$$

where C, D, and E are treated as constants found by numerical fitting. The value of P_c corresponds to the value reached by P when T is equal to T_c in eq 10. An independent way to calculate the value of T_c is to apply the scaling laws for the case of γ. In the latter case, γ is related to T_c by the following expression:[46−48]

$$\gamma = F\left(1 - \frac{T}{T_c}\right)^{1.26} \quad (11)$$

In eq 11, F and T_c are treated as unknown constants, which are found by fitting the interfacial tension data with temperature.

3. THEORY OF INTERFACIAL PROPERTIES

For a complete survey of the semiempirical approaches to calculate γ, the reader is directed to Chapter 12 from

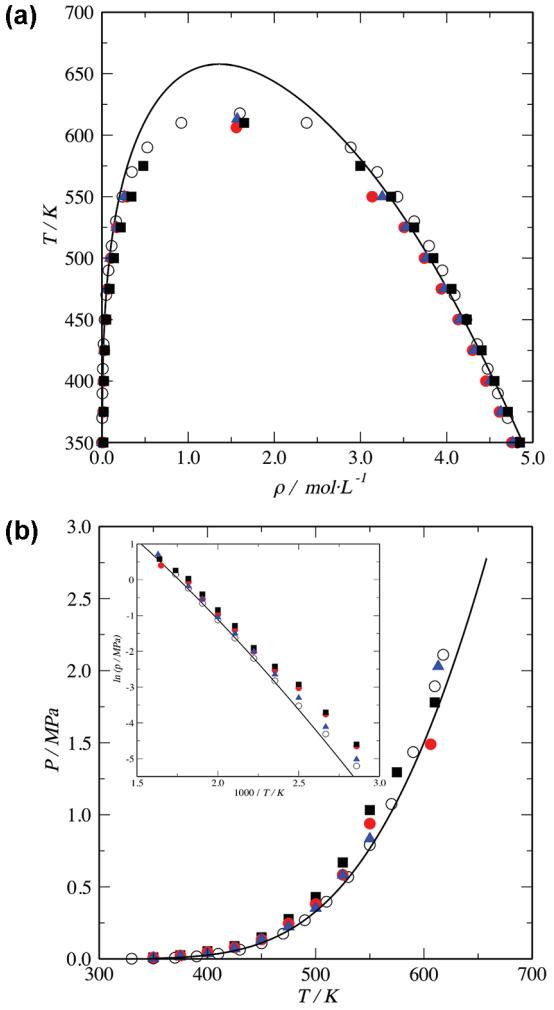

Figure 1. Phase equilibrium for *n*-decane (*n*-C_{10}). (a) coexistence densities ($\rho-T$ projection), (b) vapor pressure ($T-P$ projection). (○) experimental data[4]; (—) LJ-Chain EoS calculations; MD results for (red solid circle) NERD potential, (■) TraPPE potential, (blue solid triangle) SKS potential.

Poling et al.'s book[49] and Chapter 8 from Xiang's book.[46] Some of the most widespread semiempirical approaches for determining interfacial tensions are the corresponding states principia, the scaling law method, and the group contribution schemes. In the corresponding states method, the critical temperature (T_c) and the critical pressure (P_c) or the critical volume (V_c) of the pure fluid are used to reduce the interfacial tension, γ. The most popular dimensionless groups ($\gamma/P_c^{2/3}T_c^{1/3}$) or ($\gamma V_c^{2/3}/T_c$) are then correlated with $1 - T/T_c$ using some molecular shape information as the acentric factor. For the case of *n*-alkanes, some representative examples of such correlations are the one-reference fluid model proposed by Brock and Bird[50] and models which interpolate between two[51] or more[52] reference fluids. These models have been successfully applied to calculate γ in a broad range of *n*-alkanes (from C_2H_6 to $C_{26}H_{54}$). Scaling laws models are based on the vanishing of γ of the critical point. In these models, γ is related to the temperature by a universal exponent (~1.26)[47] and a substance-dependent parameter, cf. eq 11. In order to extend the scaling laws approach, far from the critical region, some authors (see for instance Miqueu et al.[53] and references therein) have applied Wegner's expansion[54] in powers of $(1 - T/T_c)^n$ to correct the scaling exponent of γ. The latter methodology has successfully been tested from CH_4 to C_8H_{18}. A more empirical (although surprisingly accurate) route is to recognize that the ratio of the IFT to the fourth power of the density difference between coexisting phases is a substance specific constant, denoted the Parachor.[55] The Parachor method and some modified versions (see Escobedo and Mansoori[56] and references therein) have been applied to calculate γ for a wide range of *n*-alkanes (from CH_4 to $C_{20}H_{42}$), and inspire some of the empirical relationships between γ and the molecular weight of the alkanes (see Dee and Sauer[57]). Notwithstanding the accuracy of the semiempirical approaches (typical absolute deviation within ~3 to 10% for the case of *n*-alkanes), these methods exhibit some limitations, namely they are incapable of proving information about the interfacial structure (e.g., density along the interfacial region). More importantly, the empirical nature of these correlations precludes the confident extrapolation e.g. to *n*-alkanes larger than *n*-eicosane.

The limitations mentioned above may be overcome by methodologies based on fundamental theories. One of the most versatile theories for both pure fluids and multicomponent fluid mixtures is the square gradient theory (SGT) for fluid interfaces.[48,58−61] Possibly one of its most interesting aspects is that the same equation of state (EoS) can be used to model, simultaneously and accurately, both phase equilibrium and interfacial properties. For the case of *n*-alkanes, this theory has been combined with cubic type EoS[60−69] as well as molecular-based EoS[21,24,69−72] showing an excellent performance for correlating and/or predicting interfacial properties in a wide range of temperatures, pressures, and concentrations. However, the main advantage of the molecular based EoS over cubic EoS is their enhanced capability to predict accurately the saturation densities, which are the boundaries of the interfacial region. For the case of chain fluids, as *n*-alkanes, an appropriate choice is the Lennard-Jones chain (LJ-Chain) EoS proposed by Johnson et al.[73] This EoS is an extension of the Lennard-Jones EoS for spheres[74] employing Wertheim's first order perturbation theory of polymerization.[75] This EoS is included as a part of some SAFT models[76] and has been extensively used for describing the behavior of pure fluids as well as mixtures in broad spectrum of thermo-physical conditions. Specific details related to the LJ-Chain EoS as well as SAFT EoS have been broadly summarized in refs 77−83. As the SGT and LJ-Chain EoS are well documented, in this section we only briefly summarize the main equations used in this work to calculate the phase equilibrium and its interfacial properties for pure fluids.

3.1. Square Gradient Theory for Pure Fluid Interfaces. Consider a pure liquid in equilibrium with its vapor. In this case, the liquid and vapor coexisting bulk fluid phases are connected by an interfacial fluid, whose density ρ, varies spatially between its bulk fluid phases. For the case of a planar interface, van der Waals in 1894[58] related ρ as a function of a spatial coordinate z by considering that the inhomogeneous Helmholtz energy density for a pure liquid in equilibrium with its vapor could be expressed as a Taylor expansion about the homogeneous Helmholtz energy density. The final expression is then constrained to the condition of minimum Helmholtz energy density. Mathematically, the interfacial density profile, $\rho(z)$, for the case of pure fluids is given implicitly by the following expression (see details in refs 21 and 60−64.):

$$z = z_0 + \frac{1}{\sqrt{2}}\int_{\rho_0}^{\rho(z)} \frac{\sqrt{c}}{\sqrt{\Omega + P^0}}\, d\rho \qquad (12)$$

Table 1. Phase Equilibria from Molecular Dynamics for *n*-Decane (n-C_{10})[a]

	experimental[b]		SKS			NERD			TraPPE		
T	P	ρ_L	P	ρ_V	ρ_L	P	ρ_V	ρ_L	P	ρ_V	ρ_L
K	MPa	mol L^{-1}	MPa	mol L^{-1}	mol L^{-1}	MPa	mol L^{-1}	mol L^{-1}	MPa	mol L^{-1}	mol L^{-1}
350	0.005	4.826	0.006_6	0.002_7	4.766_9	0.009_5	0.010_2	4.756_3	0.010_1	0.016_4	4.850_6
375	0.013	4.696	0.016_4	0.008_1	4.628_9	0.023_2	0.013_2	4.612_4	0.024_6	0.019_3	4.710_2
400	0.029	4.562	0.036_8	0.013_2	4.503_7	0.048_5	0.017_3	4.455_1	0.053_6	0.023_2	4.554_6
425	0.059	4.414	0.071_1	0.023_6	4.317_7	0.079_5	0.027_7	4.300_8	0.088_8	0.033_1	4.406_1
450	0.111	4.253	0.134_7	0.038_3	4.147_5	0.134_1	0.044_5	4.132_3	0.149_5	0.048_6	4.231_6
475	0.195	4.082	0.223_1	0.061_8	3.969_5	0.246_2	0.067_3	3.937_9	0.276_6	0.088_2	4.056_1
500	0.325	3.906	0.351_1	0.096_1	3.758_7	0.380_6	0.103_9	3.742_3	0.429_8	0.138_7	3.845_8
525	0.516	3.717	0.581_2	0.169_1	3.524_5	0.583_5	0.170_9	3.505_9	0.668_9	0.217_5	3.623_2
550	0.788	3.491	0.833_8	0.259_9	3.252_7	0.938_7	0.284_3	3.135_9	1.032_8	0.341_1	3.355_6
575	1.161	3.183							1.295_3	0.479_4	2.997_8
			Dev P[c]	0.024	AAD ρ_L[c]	3.01%	Dev P[c]	0.045	AAD ρ_L[c]	3.83%	Dev P[c]	0.083	AAD ρ_L[c]	1.60%

[a] Systems comprised of 780 molecules. The subscripted number is the uncertainty in the last digit. (i.e., 4.766_9 means 4.766 ± 0.0009). [b] Interpolated experimental data taken from DECHEMA.[4] [c] DevP = $(1/N_{exp})\Sigma_i^{N_{exp}}|P_i^{exp} - P_i^{cal}|$; AAD $\rho_L = (100/N_{exp})\Sigma_i^{N_{exp}}|\rho_i^{exp} - \rho_i^{cal}|/\rho_i^{exp}$.

In eq 12, z_0 is a reference spatial coordinate, the bulk density is ρ_0, P^0 is the bulk equilibrium pressure (or vapor pressure), ρ is the inhomogeneous or interfacial molar density, c is the influence parameter, and Ω is the grand thermodynamic potential, which is defined for a pure fluid as

$$\Omega = \frac{A}{V} - \rho\left(\frac{\partial A}{\partial n}\right)^0_{T,V} = \frac{A}{V} - \rho\mu^0 \tag{13}$$

In the previous equation, A is the Helmholtz energy of the homogeneous system, V is the volume, n is the mass in moles, T is the absolute temperature, μ is the chemical potential, and the superscript 0 denotes that this term is evaluated at the phase equilibrium condition of the bulk phases. Equation 13 is physically constrained by the following conditions in the bulk phases:[61,84]

$$\Omega = \Omega^0 = -P^0 \tag{14.a}$$

$$\left(\frac{\partial\Omega}{\partial\rho}\right)_{T^0,V^0} = \mu - \mu^0 = 0 \tag{14.b}$$

$$\left(\frac{\partial^2\Omega}{\partial\rho^2}\right)_{T^0,V^0} > 0 \tag{14.c}$$

Equations 14.a−c can be related to the necessary conditions of isothermal phase equilibrium for bulk phases. Specifically, eq 14.a corresponds to the mechanical equilibrium condition ($P^0 = P^L = P^V$), and eq 14.b expresses the chemical potential constraint ($\mu^0 = \mu^L = \mu^V$). Equation 14.c is a differential stability condition for interfaces, comparable to the Gibbs energy stability constraint of a single phase.[84,85]

In the context of van der Waals theory, γ can be calculated from the following integral expression:[48,60−62]

$$\gamma = \int_{-\infty}^{\infty} c\left(\frac{d\rho}{dz}\right)^2 dz \tag{15}$$

The integral limits describe the boundary conditions of bulk fluid phases, i.e, $\rho(z = -\infty) = \rho^V$ and $\rho(z = +\infty) = \rho^L$ where the superscripts V and L correspond to the molar density in the vapor and the liquid bulk phases, respectively. Replacing eq 12 in eq 15, γ can be alternatively calculated from

$$\gamma = \sqrt{2}\int_{\rho^V}^{\rho^L}\sqrt{c}\sqrt{\Omega + P^0}\, d\rho \tag{16}$$

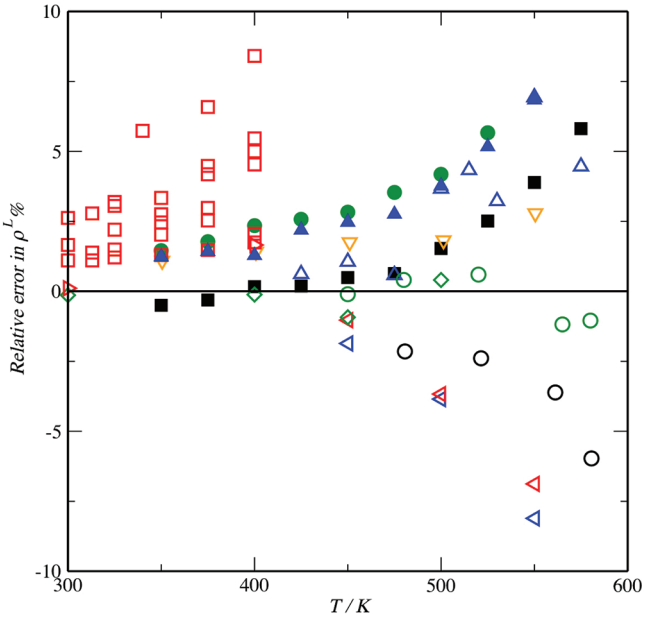

Figure 2. Relative error with respect to experimental data of the saturated liquid density of *n*-decane (n-C_{10}) as a function of temperature. This work: (green solid circle) NERD potential, (■) TraPPE potential, (blue solid triangle) SKS potential. Reported MC simulations: (blue open triangle) Smit et al.,[8] (green open circle, ○) Nath et al.,[9] (down pointing orange open triangle) Biscay et al.[19] Reported MD simulations: (right pointing red open triangle) Harris,[12] (left pointing blue open triangle, left pointing red open triangle) Nicolas and Smit,[13] (green open diamond) López-Lemus et al.,[15] (red open square) Ismail et al.,[17] (colors: green for NERD, black for TraPPE, blue for SKS, red for OPLS, and orange for anisotropic UA).

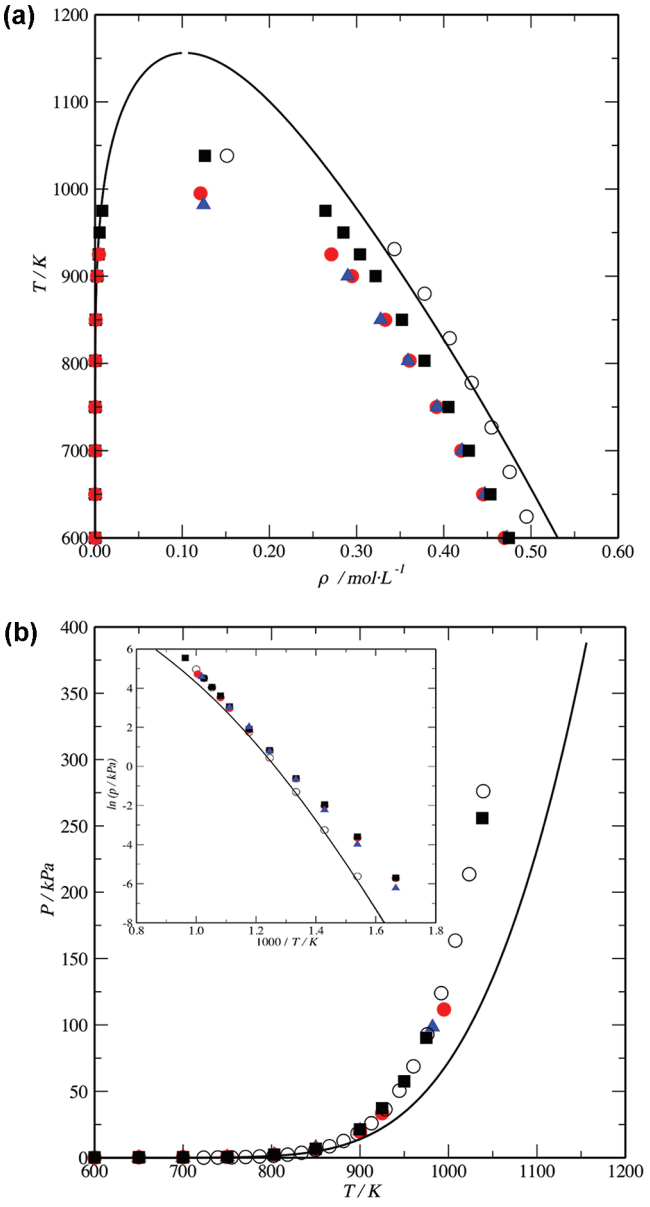

Figure 3. Phase equilibrium for *n*-decacontane (*n*-C_{100}). (a) Coexistence densities ($\rho-T$ projection), (b) vapor pressure ($T-P$ projection). (○) Recommended data;[4] (—) LJ-Chain EoS calculations; MD results for (red solid circle) NERD potential, (■) TraPPE potential, (blue solid tirangle) SKS potential.

Finally, the values of γ as a function of the saturation temperature given by eq 16 can be used to calculate other interfacial properties such as the surface entropy (Δs^{γ}) and the surface enthalpy (Δh^{γ}) change of surface formation. Δs^{γ} and Δh^{γ} can be calculated from the following derivative expressions:[48,85]

$$\Delta s^{\gamma} = -(\partial\gamma/\partial T)_{\mathrm{p}}; \quad \Delta h^{\gamma} = \gamma + T\Delta s^{\gamma} \tag{17}$$

Inspection of eqs 12−17 reveals that the calculation of $\rho(z)$, γ, and its derivatives depend on the EoS model and crucially, on the undetermined parameter *c*. It is this parameter that must be fitted to data, and the reason why SGT is not a fully predictive theory.

3.2. Lennard−Jones Chain EoS. The role of a specific EoS is to provide an analytical relation for *A* which is needed to evaluate Ω (see eq 13). Ω is then used in eqs 14 to predict the bulk equilibrium state, and in eqs 12 and 16 to calculate $\rho(z)$ and γ, respectively. The LJ-Chain EoS describes chain-like fluids as freely jointed tangent Lennard-Jones spheres, which can be taken as a coarse grained model for *n*-alkanes.

According to Johnson et al.,[73] *A* is given by the following expression:

$$A(\rho,T) = A^{\mathrm{ig}} + A^{\mathrm{r}} = nk_{\mathrm{B}}T\{\ln(\rho N_{\mathrm{av}}\Lambda^3) - 1\} + \{A_{\mathrm{R}}^{\mathrm{r}} + nk_{\mathrm{B}}T(1-m)\ln g_{\mathrm{LJ}}(\sigma)\} \tag{18}$$

where A^{ig} is the ideal gas reference and A^{r} is the residual Helmholtz energy. A^{r} is formed of two additive contributions to the Helmholtz energy: The first part is the residual Helmholtz energy for the monomeric or spherical reference fluid ($A_{\mathrm{R}}^{\mathrm{r}}$), which is given by the Lennard-Jones EoS for spheres.[74] The second part is the bonding chain contribution which is descried by the pair correlation function $g_{\mathrm{LJ}}(\sigma)$. In this EoS model, $g_{\mathrm{LJ}}(\sigma)$ is given by an empirical fitting function:

$$g_{\mathrm{LJ}}(\sigma) = 1 + \sum_{i=1}^{5}\sum_{j=1}^{5} a_{ij}(\rho N_{av}\sigma^3)^i(k_{\mathrm{B}}T/\varepsilon)^{1-j} \tag{19}$$

where a_{ij} are the fitting constants tabulated by Johnson et al.[73] The remaining terms present in eqs 18 and 19 are defined as follows: k_{B} is Boltzmann's constant, N_{av} is Avogadro's constant, Λ is the de Broglie wavelength, *m* is the molecular chain length (or number of segments), ε is the Lennard-Jones energy parameter of the interaction, and σ is the Lennard-Jones size parameter. Note that in this representation the EoS model considers the fluid to be composed of a chain of *m* tangent (bond length, σ) homonuclear beads, in contrast with the UA description where each site corresponds physically to either a CH_3 or CH_2 group; that is, there is no mapping between the EoS parameters and the UA parameters. In the case of the LJ-Chain EoS, *m* needs not be an integer number and neither does it match the carbon number. In this work, *m*, ε, and σ of the EoS are fitted to the DECHEMA recommended experimental data[4] for liquid density (or volume) and vapor pressure of long alkanes (For specific details related to the optimization function see ref 76 and 86−88.). Table S1 (Supporting Information) summarizes the optimized values and their average absolute deviation (AAD) for both saturated liquid density and vapor pressure. As the molecular chain length increases, the quality of the fit decreases; the sparcity of the data and the impossibility of tracing the origins of the experimental data make it difficult to extract further conclusions. The parameters presented in Table S1 have been correlated as a linear function to the molecular weight (M_{w}) of the pure alkane

$$m = 3.5333 + 0.011225M_{\mathrm{w}} \tag{20.a}$$

$$m\sigma^3 = 61.756 + 1.5184M_{\mathrm{w}} \tag{20.b}$$

$$m\varepsilon/k_{\mathrm{B}} = 850.12 + 3.9271M_{\mathrm{w}} \tag{20.c}$$

Equations 20.a−c may be applied to interpolate *m*, ε, and σ from *n*-decane ($C_{10}H_{22}$) to *n*-decacontane ($C_{100}H_{202}$). At this point is important to remark that previous implementations of the LJ-Chain EoS to describe *n*-alkanes only covered a very limited range of *n*-alkanes (up to C_8H_{18}),[76] and the transferability of these so-called "universal" molecular parameters to long *n*-alkanes is not possible.

3.3. Influence Parameter for Pure Fluids (*c*). The influence parameter, *c*, is theoretically related to the mean square range of

Table 2. Phase Equilibria from Molecular Dynamics for *n*-Eicosane (n-C_{20})[a]

experimental[b]			SKS			NERD			TraPPE		
T	P	ρ_L	P	ρ_V	ρ_L	P	ρ_V	ρ_L	P	ρ_V	ρ_L
K	kPa	mol L^{-1}	kPa	mol L^{-1}	mol L^{-1}	kPa	mol L^{-1}	mol L^{-1}	kPa	mol L^{-1}	mol L^{-1}
350	0.007	2.6571	0.019_3	0.002_2	2.6717_8	0.024_2	0.0011_1	2.6656_3	0.029_7	0.0032_8	2.6774_6
400	0.110	2.5433	0.274_1	0.002_6	2.5438_1	0.266_7	0.0012_7	2.5384_8	0.327_9	0.0039_1	2.5694_5
450	0.953	2.4221	1.845_2	0.003_3	2.4154_1	1.943_7	0.0013_7	2.4053_6	2.109_2	0.0043_1	2.4401_8
500	5.344	2.2912	10.808_8	0.005_1	2.2703_4	15.202_1	0.0024_4	2.2675_1	17.293_8	0.0069_6	2.3030_9
550	21.844	2.1518	33.723_5	0.009_1	2.1193_8	34.379_6	0.0065_8	2.1119_1	36.044_3	0.0110_1	2.1567_6
600	70.482	2.0024	88.738_3	0.019_4	1.9414_1	90.794_3	0.0179_8	1.9544_3	100.219_7	0.0198_6	1.9955_7
625	117.954	1.9213	136.086_2	0.029_6	1.8468_2	133.404_5	0.0284_4	1.8600_7	140.811_7	0.0296_5	1.9145_1
650	189.682	1.8330	202.778_3	0.045_9	1.7260_3	197.103_1	0.0418_3	1.7459_3	212.502_3	0.0454_6	1.8070_8
675	294.411	1.7339	291.293_7	0.063_2	1.6059_6	288.249_4	0.0611_7	1.6305_4	307.265_7	0.0651_1	1.7055_4
700	442.747	1.6192	405.501_7	0.087_3	1.4809_9				460.900_9	0.0924_6	1.5712_3
		Dev P[c]	10.82	AAD ρ_L[c]	3.19%	Dev P[c]	8.10	AAD ρ_L[c]	2.26%	Dev P[c]	13.39	AAD ρ_L[c]	1.00%

[a] Systems comprised of 409 molecules. The subscripted number is the uncertainty in the last digit. (i.e., 2.6717_8 means 2.6717 ± 0.00008). [b] Interpolated experimental data taken from DECHEMA.[4] [c] Dev $P = (1/N_{exp})\Sigma_i^{N_{exp}}|P_i^{exp} - P_i^{cal}|$; AAD $\rho_L = (100/N_{exp})\Sigma_i^{N_{exp}}|\rho_i^{exp} - \rho_i^{cal}|/\rho_i^{exp}$.

Table 3. Phase Equilibria from Molecular Dynamics for *n*-Hexacontane (n-C_{60})[a]

experimental[b]			SKS			NERD			TraPPE		
T	P	ρ_L	P	ρ_V	ρ_L	P	ρ_V	ρ_L	P	ρ_V	ρ_L
K	kPa	mol L^{-1}	kPa	mol L^{-1}	mol L^{-1}	kPa	mol L^{-1}	mol L^{-1}	kPa	mol L^{-1}	mol L^{-1}
500	5.1×10^{-5}	0.8750	0.001_1	0.0001_3	0.8486_1	0.001_2	0.0001_3	0.8417_7	0.001_3	0.0001_5	0.8495_1
550	0.002	0.8450	0.010_3	0.0001_4	0.8072_5	0.005_1	0.0001_5	0.8024_3	0.005_1	0.0001_6	0.8110_2
600	0.023	0.8132	0.092_5	0.0001_7	0.7639_9	0.020_1	0.0001_7	0.7600_1	0.021_6	0.0001_7	0.7742_6
650	0.201	0.7796	0.517_4	0.0001_8	0.7203_8	1.519_3	0.0001_8	0.7179_6	1.795_4	0.0002_1	0.7332_9
700	1.160	0.7435	2.217_3	0.0002_7	0.6717_2	2.185_8	0.0002_6	0.6648_7	2.752_8	0.0002_9	0.6903_6
750	5.009	0.7040	6.065_3	0.0008_6	0.6193_3	5.926_3	0.0007_9	0.6203_5	6.156_6	0.0008_3	0.6437_1
800	17.269	0.6593	17.553_4	0.0023_3	0.5643_9	16.239_7	0.0030_3	0.5613_7	17.257_4	0.0027_2	0.5954_1
850	49.888	0.6071	40.628_3	0.0061_3	0.5053_2	45.984_5	0.0085_3	0.4964_4	46.316_7	0.0088_1	0.5431_4
875	80.267	0.5771				67.125_6	0.0192_4	0.4410_7	69.336_7	0.0120_7	0.5067_9
900	125.115	0.5439							104.318_9	0.0180_5	0.4671_1
		Dev P[c]	1.51	AAD ρ_L[c]	9.25%	Dev P[c]	2.37	AAD ρ_L[c]	11.38%	Dev P	3.96	AAD ρ_L[c]	7.99%

[a] Systems comprised of 150 molecules. The subscripted number is the uncertainty in the last digit. (i.e., 0.8486_1 means 0.8486 ± 0.00001). [b] Interpolated recommended data taken from DECHEMA.[4] [c] Dev $P = (1/N_{exp})\Sigma_i^{N_{exp}}|P_i^{exp} - P_i^{cal}|$; AAD $\rho_L = (100/N_{exp})\Sigma_i^{N_{exp}}|\rho_i^{exp} - \rho_i^{cal}|/\rho_i^{exp}$.

the direct correlation function of the fluid. Unfortunately, this quantity is analytically untraceable so we recourse to calculating c using the procedure initially suggested by Carey[60−62] which has become standard practice (see refs 21, 24, 63−68, and 70−72.). In this approximation, c is considered a constant value, whose value is fitted by using experimental γ data[4−6] and eq 16. The optimized values as well as their AAD are summarized in Table S1. The interfacial tensions thus found are closer to the experimental values than those that could have been obtained by correlations such as corresponding states principia, the scaling law method, or the Parachor constants. In line with the fitting done to the EoS parameters, c is correlated as a function of the M_w

$$c = (25.653 - 158.93 \times 10^{-3} M_w + 5.9098 \times 10^{-4} {M_w}^2) \times 10^{-19} \text{ J m}^5 \text{ mol}^{-2} \quad (21)$$

The quadratic function for the c parameter is in agreement to previous works on SGT with SAFT−EoS type.[21,71]

4. RESULTS AND DISCUSSIONS

4.1. Bulk Phase Equilibrium. Decane was selected as a base case as it is widely studied as a prototypical parrafin, with several data sources for the VLE and IFT available. Figure 1, panels a and b, shows the $\rho-T$ and $T-P$ diagrams obtained from the LJ-Chain EoS and our molecular simulations results. The error bars for the MD simulations are roughly the same size as the symbols and are therefore not drawn. In these Figures we also include the experimental data recommended by DECHEMA,[4] which are in agreement with the values reported in the NIST webbook,[3] as well as the DIPPR database.[5] The EoS model, with the parameters presented in eq 20, is able to accurately correlate the experimental data from the low temperature up to the vicinity

Table 4. Phase Equilibria from Molecular Dynamics for *n*-Decacontane (n-C_{100})[a]

experimental[b]			SKS			NERD			TraPPE		
T	P	ρ_L	P	ρ_V	ρ_L	P	ρ_V	ρ_L	P	ρ_V	ρ_L
K	kPa	mol L^{-1}	kPa	mol L^{-1}	mol L^{-1}	kPa	mol L^{-1}	mol L^{-1}	kPa	mol L^{-1}	mol L^{-1}
600	1.96×10^{-4}	0.5037	0.002_1	0.0001_4	0.4723_5	$5.42_1 \times 10^{-3}$	0.0001_4	0.4697_2	$6.82_1 \times 10^{-3}$	0.0001_5	0.4746_1
650	3.61×10^{-3}	0.4852	0.018_5	0.0001_6	0.4470_6	0.025_8	0.0001_5	0.4450_1	0.027_7	0.0001_6	0.4532_7
700	0.038	0.4656	0.108_8	0.0001_8	0.4208_9	0.132_1	0.0001_8	0.4200_3	0.141_6	0.0001_9	0.4286_6
750	0.272	0.4446	0.515_9	0.0002_1	0.3921_1	0.530_6	0.0002_4	0.3917_9	0.540_1	0.0002_1	0.4052_9
803	1.551	0.4200	2.154_3	0.0003_2	0.3589_7	2.254_7	0.0003_3	0.3606_5	2.275_2	0.0003_4	0.3778_3
850	5.786	0.3954	7.589_7	0.0007_5	0.3275_7	6.418_9	0.0007_5	0.3327_6	6.770_3	0.0007_4	0.3519_9
900	19.506	0.3651	20.509_5	0.0022_7	0.2898_7	19.592_1	0.0022_4	0.2947_6	21.368_1	0.0023_4	0.3217_6
925	33.723	0.3478				33.517_1	0.0044_8	0.2709_3	37.255_4	0.0042_5	0.3039_1
950	56.298	0.3288							57.548_9	0.0052_6	0.2849_3
975	91.049	0.3078							90.325_1	0.0082_3	0.2642_9
			Dev P[c]	0.53	AAD ρ_L[c] 12.54%	Dev P[c]	0.25	AAD ρ_L[c] 13.50%	Dev P[c]	0.94	AAD ρ_L[c] 10.21%

[a] Systems comprised of 110 molecules. The subscripted number is the uncertainty in the last digit. (i.e., 0.4723_5 means 0.4723 ± 0.00005). [b] Interpolated recommended data taken from DECHEMA.[4] [c] Dev $P = (1/N_{exp})\Sigma_i^{N_{exp}}|P_i^{exp} - P_i^{cal}|$; AAD $\rho_L = (100/N_{exp})\Sigma_i^{N_{exp}}|\rho_i^{exp} - \rho_i^{cal}|/\rho_i^{exp}$.

Table 5. Predicted Critical Coordinates from VLE Simulations and Eqs 8−10[a]

	experimental[b]	SKS	NERD	TraPPE
		n-Decane (n-C_{10})		
T_c/K	617.80	613.21 (5.78%)	606.22 (1.87%)	609.99 (1.26%)
P_c/MPa	2.11	2.03 (3.67%)	1.49 (29.38%)	1.78 (15.64%)
ρ_c/mol L^{-1}	1.60	1.57 (1.92%)	1.56 (2.50%)	1.65 (3.12%)
		n-Eicosane (n-C_{20})		
T_c/K	768.00	752.97 (1.96%)	755.15 (1.67%)	767.91 (0.01%)
P_c/kPa	1174.60	914.16 (22.17%)	758.74 (35.40%)	994.42 (15.34%)
ρ_c/mol L^{-1}	0.855	0.725 (15.16%)	0.745 (12.87%)	0.756 (11.58%)
		n-Hexacontane (n-C_{60})		
T_c/K	977.95	932.68 (4.63%)	928.72 (5.03%)	966.55 (1.17%)
P_c/kPa	420.35	184.29 (56.16%)	145.82 (65.31%)	279.35 (33.54%)
ρ_c/mol L^{-1}	0.262	0.220 (15.85%)	0.214 (18.32%)	0.221 (15.65%)
		n-Decacontane (n-C_{100})		
T_c/K	1038.28	981.97 (5.42%)	994.94 (4.17%)	1038.15 (0.01%)
P_c/kPa	271.76	98.39 (63.79%)	111.72 (58.89%)	255.86 (5.85%)
ρ_c/mol L^{-1}	0.151	0.124 (17.60%)	0.121 (19.87%)	0.126 (16.56%)

[a] The number in parentheses corresponds to the average absolute deviation between the MD result and the corresponding experimental value. [b] Experimental data taken from DECHEMA.[4]

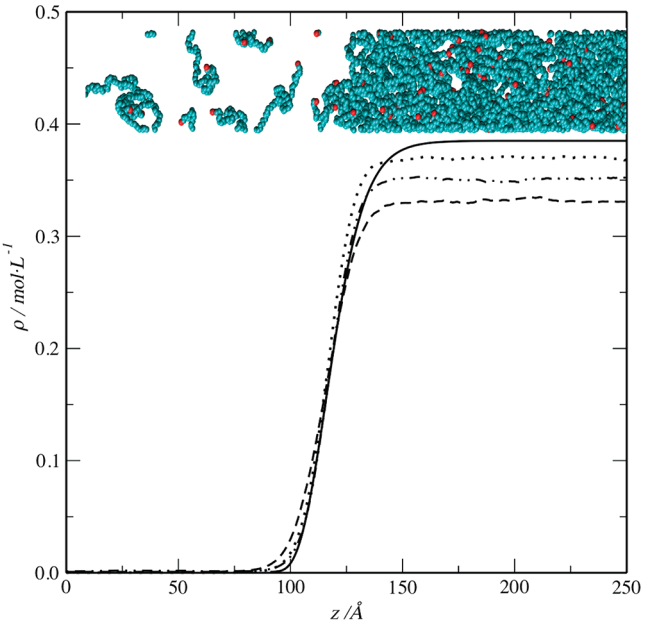

Figure 4. Interfacial density profiles for n-decacontane (n-C_{100}) at 850 K. (—) SGT + LJ-Chain EoS calculations, (· · ·) TraPPE potential, (— · · —) NERD potential, (— — —) SKS potential. Curves are displaced in z in order to match the Gibbs dividing surfaces. Insert: Snapshot of the equilibrated interfacial region 850 K. The UA groups are represented by CH_3 (red) and CH_2 (green).

of the critical state. The overprediction of the critical point is an artifact of the mean field nature of the EoS and is not of concern. It is important to draw attention to the performance of the EoS model in describing the bulk phase densities, as these are the inputs (boundary conditions) of the SGT model. In addition to Figures 1, Table 1 summarizes the numerical values of the MD results for VLE obtained from the three UA molecular potentials considered, and the corresponding statistics.

Our simulations show that all three UA potentials considered are capable of describing the reported experimental data of VLE from low temperature (~350 K) to regions close to the critical point (~550 K). Figure 1a and Table 1 showcase how the TraPPE potential results are in excellent agreement to the $\rho-T$ experimental data, the NERD and SKS potentials show moderate subpredictions of the liquid densities. The vapor phase results (see Figure 1a and Table 1) as well as vapor pressure results (see Figure 1b and Table 1) show no significant differences between TraPPE, NERD, and SKS potentials away from the critical state.

At this level of detail, simulations results should be treated in the same way as experimental data, in the sense that they are subject to uncertainties and may suffer from systematic deviations, imprecisions in the data mining, insufficient equilibration, and a host of other involuntary errors. In order to validate the results presented in Figure 1 and Table 1 with previous reports, in Figure 3 we plot the relative error in saturated liquid density as a

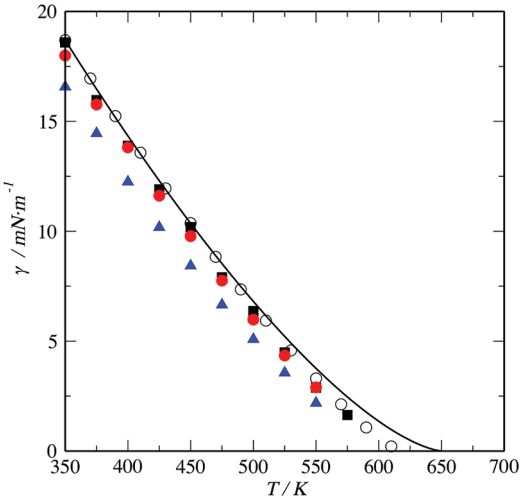

Figure 5. Interfacial tension for *n*-decane (n-C_{10}) as a function of temperature. (○) Experimental data;[4] (—) SGT + LJ-Chain EoS calculations; MD results for (red solid circle) NERD potential, (■) TraPPE potential, (blue solid triangle) SKS potential.

Table 6. Interfacial Tensions from Molecular Dynamics for *n*-Decane (n-C_{10})[a]

	γ (mN m^{-1})			
T/K	experimental[b]	SKS	NERD	TraPPE
350	18.70	16.57_2	17.99_6	18.58_9
375	16.54	14.45_1	15.76_6	15.96_5
400	14.42	12.247	13.81_3	13.88_6
425	12.35	10.18_1	11.61_7	11.90_1
450	10.35	8.42_7	9.77_4	10.18_7
475	8.43	6.65_3	7.75_2	7.90_3
500	6.61	5.08_7	5.98_2	6.36_7
525	4.90	3.55_8	4.35_1	4.48_6
550	3.33	2.18_5	2.89_8	2.88_6
575	1.89			1.64_3
	AAD γ %[c]	20.13	7.33	5.79

[a] Systems comprised of 780 molecules. The subscripted number is the uncertainty in the last digit. (i.e., 16.57_2 means 16.57 ± 0.002). [b] Interpolated experimental data taken from DECHEMA.[4] [c] AAD $\gamma = (100/N_{exp})\Sigma_i^{N_{exp}}|\gamma_i^{exp} - \gamma_i^{cal}|/\gamma_i^{exp}$.

function of temperature from other Monte Carlo[8,9,19] as well as MD[13,15,17] simulations. In spite of the significant scatter in the data, it is clear that the TraPPE model (black symbols) is the UA with the lower relative error (a maximum value of 4% near the critical state and lower than 1% at temperature lower than 525 K). Apart from the results of *n*-decane, we are aware only of two further MD points reported by Harris[12] for *n*-eicosane, both of which are in good agreement with our results.

For the other three long *n*-alkanes studied here, Tables 2−4 summarize the numerical values of the MD simulations from the UA potentials tested here and the corresponding statistical deviations. These results are also illustrated in graphical form in the Supporting Information for *n*-eicosane (Figure S1) and *n*-hexacontane (Figure S2). Figure 3 displays the VLE diagrams in both $\rho-T$ and $T-P$ projections for the longer *n*-alkane (*n*-decacontane).

Table 7. Interfacial Tensions from Molecular Dynamics for *n*-Eicosane (n-C_{20})[a]

	γ (mN m^{-1})			
T/K	experimental[b]	SKS	NERD	TraPPE
350	24.13	21.83_8	22.82_5	24.10_1
400	20.09	18.22_8	19.54_4	20.21_9
450	16.24	14.48_4	16.13_9	16.13_6
500	12.64	11.23_5	12.75_3	12.71_1
550	9.34	8.43_1	9.34_3	9.44_9
600	6.39	5.51_5	6.44_4	6.50_7
625	5.07	4.47_8	5.10_5	5.08_3
650	3.87	3.18_1	3.79_9	3.99_1
675	2.77	2.00_4	2.80_5	2.88_7
700	1.81	1.09_9		1.89_5
	AAD γ %[c]	16.05	1.55	1.72

[a] Systems comprised of 409 molecules. The subscripted number is the uncertainty in the last digit. (i.e., 21.83_8 means 21.83 ± 0.008). [b] Interpolated experimental data taken from DECHEMA.[4] [c] AAD $\gamma = (100/N_{exp})\Sigma_i^{N_{exp}}|\gamma_i^{exp} - \gamma_i^{cal}|/\gamma_i^{exp}$.

The VLE results indicate that for the shorter alkanes (*n*-decane and *n*-eicosane) the TraPPE model provides an excellent agreement to the liquid density predictions. However, as the chain length increases, all UA potentials become less accurate in representing the liquid density. For the case of vapor pressure of alkanes, the three tested UA potentials (TraPPE, NERD, and SKS) show small, but noticeable deviations from recommended data. It is important to point out that as the molecular chain increases, the capability of the UA potentials to predict VLE decreases.

In fact, while the three UA models are overall able to predict the measured experimental behavior for the liquid densities and the vapor pressures for the case of n-decane and n-eicosane, for n-hexacontane and n-decacontane, the UA potentials always exhibit subpredictions for the liquid densities and overprediction of the vapor pressure. On a speculative note, we presume that for these very long alkanes, unique contributions to the thermodynamics of the systems arise, mainly due to intramolecular interactions, the relative lack of importance of the CH_3 end groups, and in general, the polymer-like behavior of the chains. It seems unlikely that a unique set of molecular parameters can be used for the complete alkane series.

MD results are also used together with eqs 8−10 to predict the critical coordinates for the long *n*-alkanes. The critical coordinates have been included in Figures 1, 3, S1, and S2, and their numerical values are summarized in Table 5. The results from the TraPPE potential are closer to the experimental data than the other two UA potentials; the NERD and SKS potentials always subpredict the critical point.

The value of the cutoff radius has a profound effect on the outcome of the simulations, as a very short cutoff effectively corresponds to a different potential energy curve. For the case of TraPPE and NERD potentials, phase equilibrium and interfacial tensions (see next section) were calculated using a cutoff radius of 24 Å (~6 σ), where densities (liquid and vapor), vapor pressure and interfacial tension show stable values (see refs 34−38. for a complete discussion of truncation effects). For the case of SKS potential, a cutoff radius of 24 Å significantly overpredicts phase equilibrium and interfacial tension; cf. Figures S3 in the

Table 8. Interfacial Tensions from Molecular Dynamics for *n*-Hexacontane (n-C_{60})[a]

	γ (mN m^{-1})			
T/K	experimental[b]	SKS	NERD	TraPPE
500	17.49	16.96_3	19.08_5	18.73_6
550	15.27	14.51_8	15.51_1	15.98_4
600	13.11	11.88_5	13.60_9	13.39_8
650	11.02	9.70_2	10.50_1	11.28_2
700	9.00	7.96_2	8.22_9	9.01_5
750	7.07	6.13_5	5.69_2	7.32_8
800	5.23	4.55_4	4.11_3	5.34_8
850	3.49	3.01_5	2.52_2	3.51_4
875	2.66		1.98_8	2.82_7
900	1.87			2.12_9
	AAD γ %[c]	10.07	13.52	4.31

[a] Systems comprised of 150 molecules. The subscripted number is the uncertainty in the last digit. (i.e., 16.96_3 means 16.96 ± 0.003). [b] Interpolated recommended data taken from DECHEMA[4] [c] *AAD* $\gamma = (100/N_{exp})\Sigma_i^{N\ exp}|\gamma_i^{exp} - \gamma_i^{cal}|/\gamma_i^{exp}$

Table 9. Interfacial Tensions from Molecular Dynamics for *n*-Decacontane (n-C_{100})[a]

	γ (mN m^{-1})			
T/K	experimental[b]	SKS	NERD	TraPPE
600	13.64	12.62_3	13.36_8	14.54_8
650	11.76	10.43_1	11.30_3	12.50_4
700	9.93	8.55_4	9.33_9	10.37_4
750	8.16	6.51_1	7.62_9	8.50_3
803	6.37	4.92_4	5.95_3	6.56_3
850	4.86	3.50_2	4.49_2	4.80_3
900	3.33	2.00_6	3.13_4	3.38_7
925	2.60		2.40_1	2.69_1
950	1.89			2.01_1
975	1.21			1.38_4
	AAD γ %[c]	20.45	5.72	5.22

[a] Systems comprised of 110 molecules. The subscripted number is the uncertainty in the last digit. (i.e., 12.62_3 means 12.62 ± 0.003). [b] Interpolated recommended data taken from DECHEMA.[4] [c] AAD $\gamma = (100/N_{exp})\Sigma_i^{N_{exp}}|\gamma_i^{exp} - \gamma_i^{cal}|/\gamma_i^{exp}$.

Supporting Information. For the latter potential, we use of 13.8 Å, which is the value used for its parametrization.[8] See Figures S3, for a direct comparison of both cutoff radii in phase equilibrium.

4.2. Interfacial Properties. For pure fluids, MD and SGT allow the calculation of density profiles across the liquid−vapor interface, $\rho(z)$. These profiles exhibit a hyperbolic shape that spans from the vapor and liquid bulk phases. As the details of these profiles have been extensively discussed from MD and SGT approaches (see for instances refs 12, 13, 15−17, 19, 21, 32, 34−38, 41, 48, 60−63, 69−71, and 89.) we only illustrate here the $\rho(z)$ profiles for the largest hydrocarbon studied: $C_{100}H_{202}$. Figure 4 shows the $\rho(z)$ profiles obtained from the three UA potentials as well as from SGT at 850 K. Both the UA molecular potentials and SGT exhibit similar $\rho(z)$ profiles which may be fitted using tanh functions, and only small differences are noted

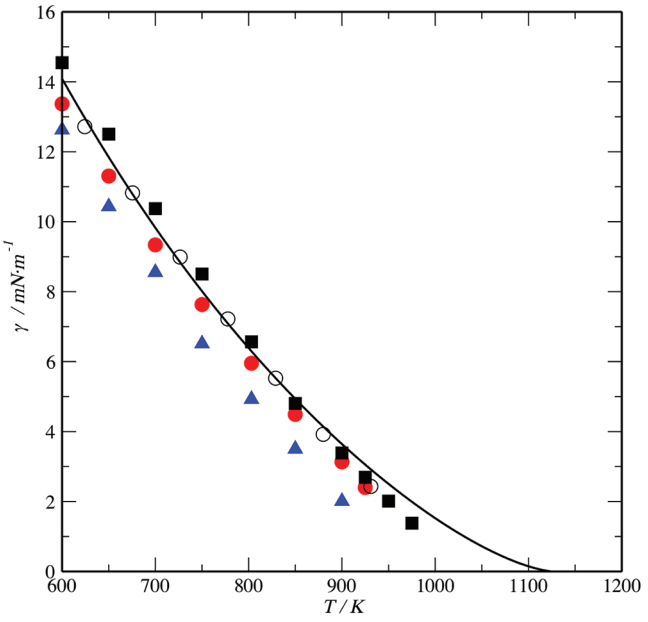

Figure 6. Interfacial tension for n-decacontane (n-C_{100}) as a function of temperature. (○) recommended data;[4] (—) SGT + LJ-Chain EoS calculations; MD results for (red solid circle) NERD potential, (■) TraPPE potential, (blue solid triangle) SKS potential.

in the different bulk densities which relate to the results of the bulk phase equilibria (Figure 3.a). Applying the 10/90 criteria proposed by Lekner and Henderson,[90] the interfacial thickness for $C_{100}H_{202}$ at 850 K gives an approximate value of 26 Å. This value will increase or decrease as the temperature increases or decreases, respectively, diverging at the critical point, where the interfacial region and interfacial tension disappear. In order to illustrate this effect, Figure S4 (in the Supporting Information) shows the $\rho(z)$ profiles at 600, 750, and 925 K where the interfacial thicknesses correspond to values of 11.44 Å, 16.10 Å and 46.63 Å respectively.

The insert of Figure 4 shows a snapshot of the interfacial region of a corresponding equilibrated configuration at 850 K. In this snapshot, it is possible to observe the bulk phases (liquid and vapor), the interfacial region, its "rugosity" and the relative position of the methyl (CH_3−) and ethyl (CH_2−) groups that conform the $C_{100}H_{202}$. No significant orientation of the molecules at the interface was observed.

Figure 5 (data in table 6) shows the thermal variation of the interfacial tension (IFT) for decane including the experimental data recommended by DECHEMA,[4] the calculations from SGT + LJ-Chain EoS, and the MD results using the SKS, NERD, and TraPPE UA potentials. SGT results show a good correlation of the interfacial tension from low temperature to high temperature. In the proximity of the critical point, SGT overpredicts the $T-\gamma$ behavior as it follows the overestimation of the critical state from the LJ-Chain EoS. All three UA potentials are able to capture the $T-\gamma$ curvature, but only NERD and TraPPE UA potentials match the experimental data, the latter having the closest fit, while the SKS potential follows an outlying behavior (AADγ > 20%). In Figure S5 (Supporting Information), we plot the relative error in γ as a function of temperature from our results as compared to reported other Monte Carlo[16,19] as well as MD[12,13,17,18] simulations. The dispersion of the data, analogous to that seen for the

Table 10. Predicted Critical Temperature Extrapolated from Interfacial Tension Simulations and Eq 11[a]

	experimental[b]	SKS	NERD	TraPPE
		n-Decane (*n*-C_{10})		
T_c/K	617.80	596.97 (3.37%)	609.18 (1.40%)	611.18 (1.07%)
		n-Eicosane (*n*-C_{20})		
T_c/K	768.00	731.51 (4.75%)	746.07 (2.86%)	743.29 (3.22%)
		n-Hexacontane (*n*-C_{60})		
T_c/K	977.95	959.50 (1.88%)	930.99 (4.80%)	979.83 (0.19%)
		n-Decacontane (*n*-C_{100})		
T_c/K	1038.28	988.46 (4.80%)	1035.28 (0.29%)	1043.78 (0.53%)

[a] The number in parentheses corresponds to the average absolute deviation between the MD result and the corresponding experimental value. [b] Experimental data taken from DECHEMA.[4]

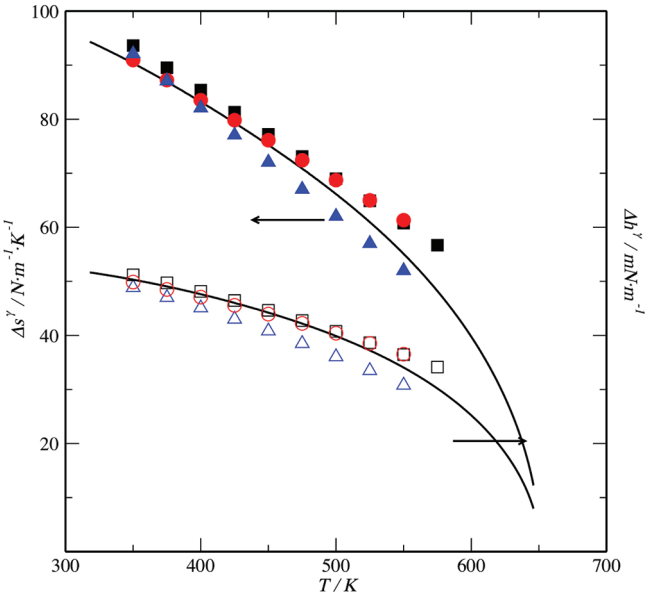

Figure 7. Variation of surface entropy (Δs^{γ}) and surface enthalpy (Δh^{γ}) with the temperature for *n*-decane (*n*-C_{10}). (—) SGT + LJ-Chain EoS calculations; MD results of Δs^{γ} for (red solid circle) NERD potential, (■) TraPPE potential, (blue solid triangle) SKS potential; MD results of Δh^{γ} for (red open circle) NERD potential, (□) TraPPE potential, (blue open triangle) SKS potential.

densities (cf. Figure 2) give a measure of the uncertainty in the simulation data.

For the other three *n*-alkanes studied, Tables 7−9 summarize the numerical values of the MD simulations from the UA potentials tested here and the corresponding statistical deviations. These results are also illustrated in the Supporting Information for *n*-eicosane (Figure S6a) and *n*-hexacontane (Figure S6b) and in Figure 6 the longer *n*-alkane (*n*-decacontane).

It is seen in Tables 6−9 and Figures 5, 6, and S6 that the MD results from TraPPE model give the closest match to the experimental data, whereas the SKS potential is unable to correctly model the interfacial tension behavior.

In addition to these IFT results, $T-\gamma$ behavior was evaluated using two cutoff radii for the SKS potentials. In Figures S7 (Supporting Information), it is possible to observe that larger cutoff radius produces a significantly overprediction of IFT. The observed overestimation of the IFT from SKS potential has been also reported before by Ismail et al.,[17] for the case of *n*-eicosane.

The knowledge of the $T-\gamma$ relationship can be also used to estimate the critical temperature from scaling laws (see eq 11). The estimated values of critical temperature from eq 11 are summarized in Table 10 and match experimental data with good accuracy, particularly those obtained using the TraPPE and NERD model. The IFT isotherms can also be used predict related interfacial properties such as the surface entropy (Δs^{γ}) and the surface enthalpy (Δh^{γ}) change of surface formation (see eq 17). Figure 7 shows the behavior of Δs^{γ} and Δh^{γ} for the case of *n*-decane. Both derivative properties decrease as the temperature increases, as is expected due to the gradual disappearance of the interface as the temperature increases. While no experimental data of this kind exist, the MD simulations are able to capture the curvature of $T - \Delta s^{\gamma}$ and $T - \Delta h^{\gamma}$ curves predicted from SGT. The scatter in the data can be attributed to the numerical imprecision caused by the first order forward derivate scheme used. Further graphs of Δs^{γ} and Δh^{γ} for *n*-eicosane, *n*-hexacontane, and *n*-decacontane are included in the Supporting Information (see Figures S8−S10). These figures show similar patterns than *n*-decane. It is interesting to note that at fixed temperature, the values of Δs^{γ} and Δh^{γ} do not show significant molecular chain dependence.

5. CONCLUDING REMARKS

Recapping, the main objective of this work is to compare and critically evaluate the prediction of phase equilibria and interfacial properties for pure long *n*-alkanes fluids obtained from MD using the most commonly employed UA forcefields. The simulations were compared among themselves and to EoS, SGT calculations, and experimental or recommended data, obtained from the open literature with no prejudgement on their accuracy.

As an ancillary contribution, we propose a new set of the molecular parameters for LJ-Chain EoS (m, ε, and σ parameters), as well as for SGT (c parameter), which yield accurate results for both phase equilibrium (vapor pressure and liquid and vapor densities) and interfacial properties (density profiles along the interfacial region, interfacial tensions, the surface entropy, and the surface enthalpy change of surface formation). The new set of the molecular parameters extend the capability of the SGT with the LJ-Chain approach to describe the VLE and interfacial properties for heavy hydrocarbons ranking from *n*-decane to *n*-decacontane.

All three tested UA potentials are capable of describing the bulk phase equilibrium (VLE) and the interfacial tension (IFT) with a relatively low absolute average deviation values with respect to the experimental data, but fine issues with respect to the transferability and representability are seen, noticeably, for the longer chains, as it becomes obvious that other physical phenomena, possibly intramolecular interactions, flexibility and the lower relative contribution of the end groups become important issues. There may not be any unique parameter set that optimally represents UA groups of alkanes in both small (<C_{10}) and long chains. Although only marginally, the performance of the present TraPPE model appears superior to the NERD and SKS potential in its application to model simultaneously bulk and interfacial properties and to estimate the critical properties for long-chained n-alkanes.

■ ASSOCIATED CONTENT

Supporting Information. Table S1 summarizes the set of molecular parameters: molecular chain length (m), the Lennard-Jones energy (ε), Lennard-Jones size (σ), and influence parameter (c) for the LJ-Chain EoS and SGT for n-alkanes, and their deviations. Figure S1 and S2 show the phase equilibria for *n*-eicosane and *n*-hexacontane in (a) $\rho-T$ and (b) $T-P$ (b) projections. Figures S3 show the effect of cutoff radius in SKS potential for phase equilibria for the hydrocarbons studied here. Figure S4 shows the $z-\rho$ profiles and the corresponding interfacial thickness obtained from the SKS potential for *n*-decacontane at 600, 750, and 925 K. Figure S5 presents the relative error in interfacial tension for *n*-decane calculated in this work as compared to simulation results from the literatura. Figures S6 shows the interfacial tension for *n*-eicosane (Figure S6.a) and *n*-hexacontane (Figure S6.b) as a function of temperature. Figure S7 shows the effect of the cutoff radius in the SKS potential on the interfacial tension of the hydrocarbons studied here. Figures S8 to S10 show the variation of surface entropy and surface enthalpy with the temperature for *n*-eicosane, *n*-hexacontane, and *n*-decacontane. This material is available free of charge via the Internet at http://pubs.acs.org.

■ AUTHOR INFORMATION

Corresponding Author

*E-mail: e.muller@imperial.ac.uk; amejia@udec.cl.

Present Addresses

[†]Departamento de Ingeniería Química, Universidad de Concepción, POB 160-C, Correo 3, Concepción, Chile.

■ ACKNOWLEDGMENT

Partial financial support from U.K. Engineering and Physical Sciences Research Council through (EPSRC) Grant EP/E016340 "Molecular Systems Engineering" and FONDECYT, Santiago, Chile (Project 1080596) is gratefully acknowledged.

■ REFERENCES

(1) Danesh, A. *PVT and Phase Behavior of Petroleum Reservoir Fluids*; Elsevier: Amsterdam, 1998.
(2) Myers, D. Surfaces, Interfaces, and Colloids. *Principles and Applications*, 2nd ed.; Wiley-VCH: Berlin, 1999.
(3) Lemmon, E. W.; McLinden, M. O.; Friend, D. G. *Thermophysical Properties of Fluid Systems in NIST Chemistry WebBook*, NIST Standard Reference Database Number 69; Linstrom, P. J., Mallard, W. G., Eds.; National Institute of Standards and Technology: Gaithersburg MD; http://webbook.nist.gov; retrieved July, 2011.
(4) DECHEMA Gesellschaft für Chemische Technik und Biotechnologie e.V., Frankfurt am Main, Germany, https://cdsdt.dl.ac.uk/detherm/, (retrieved July, 2011).
(5) Daubert, T. E.; Danner, R. P. *Physical and Thermodynamic Properties of Pure Chemicals: Data Compilation*; Taylor and Francis: Bristol, PA, 1989.
(6) Wohlfarth, Ch.; Wohlfarth, B. Numerical Data and Functional Relationships in Science and Technology, Vols. 16 & 24, *Surface Tension of Pure Liquids and Binary Liquid Mixtures*; Lechner, M. D., Eds.; in Landolt-Börnstein, New Series Group IV Physical Chemistry; Springer Verlag: Berlin, 1997.
(7) Siepmann, J. I.; Karaborni, S.; Smit, B. *Nature* **1993**, *365*, 330–332.
(8) Smit, B.; Karaborni, S.; Siepmann, J. I. *J. Chem. Phys.* **1995**, *102*, 2126–2140. *J. Chem. Phys.* **1998**, *109*, 352.
(9) Nath, S. K.; Escobedo, F. A.; de Pablo, J. *J. J. Chem. Phys.* **1998**, *108*, 9905–9911.
(10) Martin, M. G; Siepmann, J. I. *J. Phys. Chem. B* **1998**, *102*, 2569–2577.
(11) Errington, J. R.; Panagiotopoulos, A. Z. *J. Phys. Chem. B* **1999**, *103*, 6314–6322.
(12) Harris., J. G. *J. Phys. Chem.* **1992**, *96*, 5077–5086.
(13) Nicolas, J. P.; Smit., B. *Mol. Phys.* **2002**, *100*, 2471–2475.
(14) Singh, J. K.; Errington., J. R. *J. Phys. Chem. B* **2006**, *110*, 1369–1376.
(15) López-Lemus, J.; Romero-Bastida, M.; Darden, T. A.; Alejandre, J. *Mol. Phys.* **2006**, *104*, 2413–2421.
(16) Ibergay, C.; Ghoufi, A.; Goujon, F.; Ungerer, P.; Boutin, A.; Rousseau, B.; Malfrey, P. *Phys. Rev. E.* **2007**, *75*, 051602–1 − 051602−18.
(17) Ismail, A . E.; Tsige, M.; Veld, P. J. IN 'T.; Grest, G. S. *Mol. Phys.* **2007**, *105*, 3155–3163.
(18) Mendoza, F. N.; López-Rendón, R.; López-Lemus, J.; Cruz, J.; Alejandre, J. *Mol. Phys.* **2008**, *106*, 1055–1059.
(19) Biscay, F.; Ghoufifi, A.; Goujon, F.; Lachet, V.; Malfreyt, P. *J. Phys. Chem. B* **2008**, *112*, 13885–13897.
(20) Amat, M. A.; Rutledge, G. C. *J. Chem. Phys.* **2010**, *132*, 114704–1 − 114704−9.
(21) Fu, D.; Li, X. S.; Yan, X. S.; Liao, T. *Ind. Eng. Chem. Res.* **2006**, *45*, 8199–8206.
(22) Chen, B.; Siepmann, J. I.; Oh, K. J.; Klein, L. L. *J. Chem. Phys.* **2002**, *116*, 4317–4329.
(23) Makrodimitri, Z. A.; Unruh, D. J. M.; Economou, I. G. *J. Phys. Chem. B* **2011**, *155*, 1429–1439.
(24) Müller, E. A.; Mejía, A. *Fluid Phase Equilib.* **2009**, *282*, 68–81.
(25) Allen, M. P.; Tildesley, D. J. *Computer Simulation of Liquids*; Clarendon: Oxford, 1987.
(26) Frenkel, D.; Smit, B. *Understanding Molecular Simulation*, 2nd ed.; Academic Press: New York, 2002.
(27) Alejandre, J.; Tildesley, D. J.; Chapela, G. A. *Mol. Phys.* **1995**, *85*, 651–663.
(28) Khare, R.; de Pablo, J. J.; Yethiraj, A. *J. Chem. Phys.* **1997**, *107*, 6956–6964.
(29) van der Ploeg, P.; Berendsen, H. J. C. *J. Chem. Phys.* **1982**, *76*, 3271–3276.
(30) Jorgensen, W. L.; Madura, J. D.; Swenson, C. J. *J. Am. Chem. Soc.* **1984**, *106*, 6638–6646.
(31) Martinez-Veracoechea, F.; Müller, E. A. *Mol. Simulat.* **2005**, *31*, 33–43.
(32) Gonzalez-Melchor, M.; Orea, P.; Lopez-Lemus, J.; Bresme, F.; Alejandre, J. *J. Chem. Phys.* **2005**, *122*, 094503–1−094503−8.
(33) Janecek, J. *J. Chem. Phys.* **2009**, *131*, 124513–1−124513−9.
(34) Holcomb, C. D.; Clancy, P.; Zollweg, J. A. *Mol. Phys.* **1993**, *78*, 437–459.
(35) Mecke, M.; Winkelmann, J.; Fischer, J. *J. Chem. Phys.* **1997**, *107*, 9264–9270.
(36) Trokhymchuk, A.; Alejandre, J. *J. Chem. Phys.* **1999**, *111*, 8510–8523.
(37) Duque, D.; Vega, L. F. *J. Chem. Phys.* **2004**, *121*, 8611–8617.
(38) Blas, F. J.; MacDowell, L. G.; de Miguel, E.; Jackson, G. *J. Chem. Phys.* **2008**, *129*, 144703–1− 144703−9.
(39) DL_POLY Molecular Simulation Package, http://www.ccp5.ac.uk/DL_POLY/. See alsoSmith, W.; Forester, T. R. *J. Molecular Graphics* **1996**, *14*, 136–141.
(40) Irving, J. H.; Kirkwood, J. G. *J. Chem. Phys.* **1950**, *18*, 817–829.
(41) Mejía, A.; Pàmies, J. C.; Duque, D.; Segura, H.; Vega, L. F. *J. Chem. Phys.* **2005**, *123*, 034505–034515.
(42) Gloor, G. J.; Jackson, G.; Blas, F. J.; de Miguel, E. *J. Chem. Phys.* **2005**, *123*, 134703−1−−134703−19.
(43) de Miguel, E.; Jackson, G. *J. Chem. Phys.* **2006**, *125*, 164109−1−−164109−11.
(44) Sampayo, J. G.; Blas, F. J.; de Miguel, E.; Müller, E. A.; Jackson, G. *J. Chem. Eng. Data* **2010**, *55*, 4306–4314.

(45) Rowlinson, J. S.; Swinton, F. L. *Liquids and Liquid Mixtures*, 3rd ed.; Butterworth: London, 1982.
(46) Xiang, H. W. The Corresponding-States Principle and its Practice Thermodynamic. *Transport and Surface Properties of Fluids*; Elsevier: Amsterdam, 2005.
(47) Widom, B. *J. Chem. Phys.* **1965**, *43*, 3892–3897.
(48) Rowlinson, J. S.; Widom, B. *Molecular Theory of Capillarity*; Oxford University Press: Oxford, 1989.
(49) Poling, B. E.; Prausnitz, J. M.; O'Connell, J. *The Properties of Gases and Liquids*, 5th ed.; McGraw-Hill: New York, 2002.
(50) Brock, J. R.; Bird, R. B. *AIChE J.* **1955**, *1*, 174–177.
(51) Zuo, Y. X.; Stenby, E. H. *Can. J. Chem. Eng.* **1997**, *75*, 1130–1137.
(52) Queimada, A. J.; Marrucho, I. M.; Coutinho., J. A. P. *Fluid Phase Equilib.* **2000**, *183−184*, 229–238.
(53) Miquie, C.; Broseta, D.; Satherley, J.; Mendiboure, B.; Lachaise, J.; Graciaa, A. *Fluid Phase Equilib.* **2000**, *172*, 169–182.
(54) Wegner, F. J. *Phys. Rev. B* **1972**, *5*, 4529–4536.
(55) MacLeod, D. B. *Trans. Faraday Soc.* **1923**, *19*, 38–43.
(56) Escobedo, J.; Mansoori, G. A. *AIChE J.* **1996**, *42*, 1425–1433.
(57) Dee, G. T.; Sauer, B. B. *Adv. Phys.* **1998**, *47*, 161–205.
(58) van der Waals, J. D. *Zeit. Phys. Chem.* **1893**, *13*, 657–725. (seeRowlinson, J. S. *J. Statist. Phys.* **1979**, *20*, 197–244for an English translation).
(59) Cahn, J. W.; Hilliard, J. E. *J. Chem. Phys.* **1958**, *28*, 258–267.
(60) Carey, B. S. *The Gradient Theory of Fluid Interfaces*, Ph.D. Thesis, University of Minnesota, 1979.
(61) Davis, H. T.; Scriven, L. E. *Adv. Chem. Phys.* **1982**, *49*, 357–454.
(62) Carey, B. S.; Scriven, L. E.; Davis, H. T. *AIChE J.* **1978**, *24*, 1076–1080. *AIChE J.* **1980**, *24*, 705–711.
(63) Cornelisse, P. M. W.; Peters, C. J.; de Swaan Arons, J. *Fluid Phase Equilib.* **1993**, *82*, 119–129. *Mol. Phys.* **1993**, *80*, 941–955. *Fluid Phase Equilib.* **1996**, *117*, 312–319.
(64) Zuo, Y. X.; Stenby, E. H. *Fluid Phase Equilib.* **1997**, *132*, 139–158.
(65) Miqueu, C.; Mendiboure, B.; Graciaa, A.; Lachaise, J. *Fluid Phase Equilib.* **2003**, *207*, 225–246.
(66) Queimada, A. J.; Miqueu, C.; Marrucho, I. M.; Kontogeorgis, G. M.; Coutinho, J. A. P. *Fluid Phase Equilib.* **2005**, *228 − 229*, 479–485.
(67) Lin, H.; Duan, Y.-Y.; Mina, Q. *Fluid Phase Equilib.* **2007**, *254*, 75–90.
(68) Oliveira, M. B.; Marrucho, I. M.; Coutinho, J. A. P.; Queimada, A. J. *Fluid Phase Equilib.* **2008**, *267*, 83–91.
(69) Nino-Amezquita, O. G.; Enders, S.; Jaeger, P. T.; Eggers, R. *Ind. Eng. Chem. Res.* **2010**, *49*, 592–601.
(70) Poser, C. I.; Sanchez, J. *J. Colloid Interface Sci.* **1979**, *69*, 539–548.
(71) Kahl, H.; Enders, S. *Fluid Phase Equilib.* **2000**, *172*, 27–42.
(72) Mejía, A.; Segura, H.; Wisniak, J.; Polishuk, I. *Phys. Chem. Liq.* **2006**, *44*, 45–59.
(73) Johnson, J. K.; Müller, E. A.; Gubbins, K. E. *J. Phys. Chem.* **1994**, *98*, 6413–6419.
(74) Johnson, J. K.; Zollweg, J. A.; Gubbins, K. E. *Mol. Phys.* **1993**, *78*, 591–618.
(75) Wertheim, M. S. *J. Chem. Phys.* **1987**, *87*, 7323–7331.
(76) Pàmies, J. C.; Vega, L. F. *Ind. Eng. Chem. Res.* **1996**, *35*, 4727–4737.
(77) Wei, Y. S.; Sadus, R. *AIChE J.* **2000**, *46*, 169–196.
(78) Müller, E. A.; Gubbins, K. E. *In Equations of State for Fluids and Fluid Mixtures*; Sengers, J. V., Kayser, R. F., Peters, C. J., White, H. J. Jr., Eds.; Elsevier: New York, 2000; pp 435−477.
(79) Müller, E. A.; Gubbins, K. E. *Ind. Eng. Chem. Res.* **2001**, *40*, 2193–2211.
(80) Economou, I. G. *Ind. Eng. Chem. Res.* **2002**, *41*, 953–962.
(81) Paricaud, P.; Galindo, A.; Jackson, G. *Fluid Phase Equilib.* **2002**, *194−197*, 87–96.
(82) Tan, S. P.; Adidharma, H.; Radosz, M. *Ind. Eng. Chem. Res.* **2008**, *47*, 8063–8082.
(83) Kontogeorgis, G. M.; Folas, G. K. *Thermodynamic models for industrial applications*: J. Wiley, U.K., 2010.
(84) Mejía, A.; Segura, H.; Vega, L. F.; Wisniak, J. *Fluid Phase Equilib.* **2005**, *227*, 225–238.
(85) Modell, M.; Tester, J. *Thermodynamics and its Applications*, 3th ed.; Prentice-Hall: New York, 1996.
(86) Huang, S. H.; Radosz, M. *Ind. Eng. Chem. Res.* **1990**, *29*, 2284–2294.
(87) McCabe, C.; Jackson, G. *Phys. Chem. Chem. Phys.* **1999**, *1*, 2057–2064.
(88) Kraska, T.; Gubbins, K. E. *Ind. Eng. Chem. Res.* **1996**, *35*, 4727–4737.
(89) Duque, D.; Pàmies, J. C.; Vega, L. F. J. *Chem. Phys.* **2004**, *121*, 11395–11401.
(90) Lekner, J.; Henderson, J. *Physica A* **1978**, *94*, 545–558.